A robust forward-displacement analysis of spherical parallel robots

Shaoping Bai [a,*], Michael R. Hansen [b], Jorge Angeles [c]

[a] Department of Mechanical Engineering, Aalborg University, 9200 Aalborg, Denmark
[b] Department of Engineering, University of Agder, Norway
[c] Department of Mechanical Engineering, McGill University, Montreal, Canada

ABSTRACT

The forward-displacement analysis of spherical parallel robots (SPRs) is revisited. A robust approach, based on the input–output (I/O) equation of spherical four-bar linkages, is proposed. In this approach, the closed-loop kinematic chain of a SPR is partitioned into two four-bar spherical chains, whose I/O equations are at the core of the analysis reported here. These equations lead to a trigonometric equation in the joint angles, which is solved semi-graphically to obtain the joint variables for the determination of the moving plate orientation. Examples are included to demonstrate the application of the method.

© 2009 Elsevier Ltd. All rights reserved.

1. Introduction

Spherical parallel robots (SPRs) are intended to provide three degrees of freedom of pure rotation. These robots have been used for applications such as camera-orienting and medical-instrument alignment [1–3]. Extensive studies have been reported for spherical parallel robots in a variety of relevant problems covering workspace modeling [4], dexterity evaluation [5], design and optimization [6–8], singularity analysis [9], and type synthesis [10], among others.

The forward-displacement analysis (FDA) of SPRs is concerned with finding the orientation of the mobile platform corresponding to a given set of actuated-joint-variable values. Due to their multi-loop architecture, the FDA of SPRs, in general, does not allow for closed-form solutions. Moreover, the nonlinear system of trigonometric equations implies a high computational complexity. It is noted that a SPR admits at most eight solutions, as reported in [11,12]. All solutions stem from the roots of an eighth-order polynomial equation, what is known as the robot *characteristic equation*.

Fig. 1 depicts two common types of SPRs, namely, 3-RRR and 3-UPU, where R, U, and P stand for revolute, universal, and prismatic joints, respectively. A SPR of the 3-RRR type has three legs, numbered from 1 to 3, each having two links and three revolute joints. The axes of all joints intersect at a common point, which is called the *center of the mechanism*. A method for the kinematics of SPRs consisting of revolute joints was reported by Gosselin et al. [12]. In this method, the orientation of the end-effector is described by means of Euler angles. Solutions in the form of an eighth-order polynomial equation were found. A similar solution was reported by Huang and Yao [13], who regarded the direction cosines of each joint axis as functions of the actuated-joint variables. In addition, Alizade et al. [14] investigated the spherical parallel robot with revolute joints, wherein a specific architecture was considered that lends itself to closed-form solutions.

---

* Corresponding author.
  E-mail addresses: shb@me.aau.dk (S. Bai), michael.r.hansen@uia.no (M.R. Hansen), angeles@cim.mcgill.ca (J. Angeles).
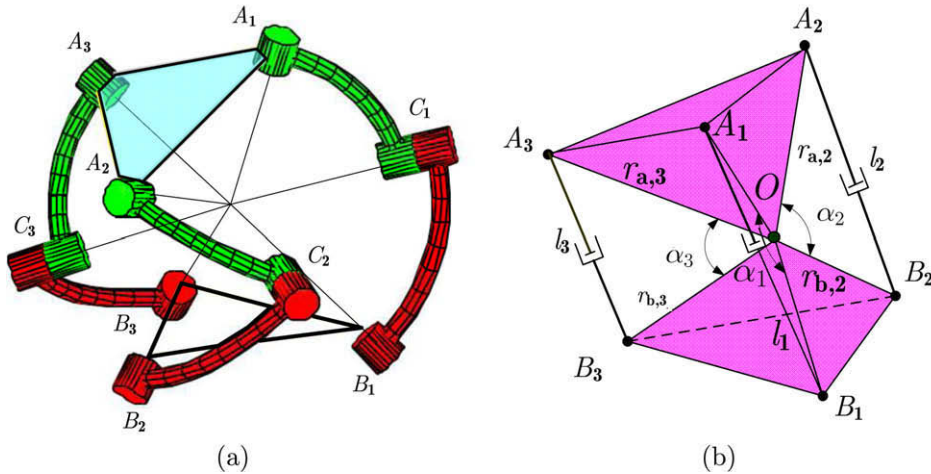
Fig. 1. Spherical parallel robots: (a) 3-RRR type, and (b) 3-UPU type.

For a SPR of the 3-UPU type,[1] as shown in Fig. 1b, the base and mobile platforms are connected through a spherical joint, located at O, the center of the robot. Three actuators for the three prismatic joints control the orientation of the end-effector. For this type of robot, Innocenti and Parenti-Castelli [11] derived a system of two equations, one eighth-order polynomial and one linear equation. In the work of Ji and Wu [15], the FDA of spherical parallel robots with prismatic joints with identical pyramids was studied by resorting to three closure equations.

It is noted from the literature that most studies were conducted for only one type of SPR, which is either 3-RRR or 3-UPU. While the kinematics solutions are mostly based on the closure equations of single legs, lengthy symbolic coefficients are involved in the kinematic equations.

In this paper, the problem of the FDA of SPRs is revisited with the aim of finding a robust method of forward-displacement analysis. A method applicable to the kinematics of spherical four-bar linkages is extended to SPRs. In the method, such a robot is considered as a multi-loop linkage made up of two spherical four-bar chains, rather than three individual legs in parallel. This approach benefits the FDA in three respects: (i) it leads to FDA equations with compact coefficients; (ii) the FDA equations can be solved semigraphically, which enhances the robustness of the analysis; and (*iii*) it is applicable to the above two types of SPR, 3-RRR and 3-UPU.

2. Problem statement

The proposed method is developed for SPRs with revolute joints. To this end, Fig. 1a is redrawn, as shown in Fig. 2, including the notation used throughout the paper. In the figure, the orientation of the axes of all joints is denoted by the unit vectors $\mathbf{u}_i$, $\mathbf{v}_i$, and $\mathbf{w}_i$, for $i = 1, 2, 3$. The coordinate system is selected such that the origin is located at the center of the mechanism, while the z-axis is normal to the bottom surface of the fixed pyramid and points upwards. The y-axis is orthogonal to the z-axis and lies in the plane made by the z-axis and $\mathbf{u}_1$. Moreover, the dimensions of the proximal links, connected to the base platform, and the distal links, connected to the mobile platform, are assumed to be α_1 and α_2, respectively[2]. Let the input joint angles be θ_i, $i = 1, 2, 3$, which are measured from the plane made by the z-axis and $\mathbf{u}_i$ to the plane of a proximal link. For the closed chain of the spherical parallel robot, we have[3]

$$\mathbf{w}_i \cdot \mathbf{v}_i = \cos \alpha_2, \quad i = 1, 2, 3 \tag{1}$$

An objective of the FDA is to find vectors $\mathbf{v}_i$. Different approaches are available for this purpose, as recalled below:

- *Using the three unit vectors of the mobile platform as unknowns*
  In this approach, the problem involves nine unknowns. Besides Eq. (1), additional equations are needed, which are

$$\mathbf{v}_i \cdot \mathbf{v}_j = \cos \alpha_3, \quad i, j = 1, 2, 3, \ i \neq j \tag{2}$$

  where α_3 is the angle between the axes of the ith and jth distal joints. The angle α_3, defined by the lateral edges of the mobile pyramid, takes the value $\alpha_3 = 2 \sin^{-1}[\sin \beta \cos(\pi/6)]$, $\alpha_3 \in (0, \pi]$. Moreover, vectors $\mathbf{v}_i$ obey

$$\|\mathbf{v}_i\| = 1 \tag{3}$$

---

[1] UPU kinematic chains can be regarded as SPS, UPS, or SPU chains as well, with S standing for spherical joints. This is possible because the extra revolute joint of a S joint becomes idle in this array.

[2] All leg-chains are assumed identical for brevity, but the method is equally applicable to general architectures.

[3] With nonidentical links, Eq. (1) becomes $\mathbf{w}_i \cdot \mathbf{v}_i = \cos \alpha_{2,i}$.
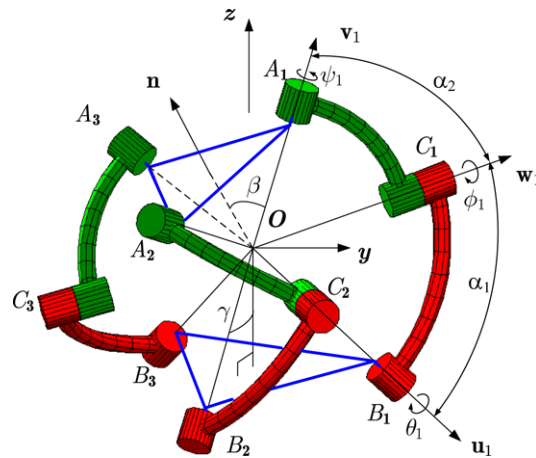
Fig. 2. Kinematic model of a spherical parallel robot.

Eqs. (1)–(3) form a system of three linear and six quadratic equations of vectors $\mathbf{v}_i$, from which possible values of $\mathbf{v}_i$ can be found. This is a general approach in dealing with the FDA of SPRs. However, the Bezout number of the system of equations is $64 (= 2^6)$, which implies a high computational complexity.

- *Using the Euler angles of the mobile platform as unknowns*

  The unit vectors $\mathbf{v}_i$ can be expressed by

$$\mathbf{v}_i = \mathbf{Q}\mathbf{v}_i^* \tag{4}$$

  where $\mathbf{Q}$ is the rotation matrix and $\mathbf{v}_i^*$ is the unit vector counterpart of $\mathbf{v}_i$, as expressed in mobile-platform coordinates. If the orientation of the mobile platform is described by the array of Euler angles $\boldsymbol{\varphi} = [\varphi_1, \varphi_2, \varphi_3]^T$, then the rotation matrix is

$$\mathbf{Q}_i = \mathbf{Q}_i(\boldsymbol{\varphi}) \tag{5}$$

  the system of three Eq. (1) thus having three unknown Euler angles. In [12], the coordinate system fixed to the mobile platform was carefully selected to simplify the equations: the z-axis was aligned with the shaft axis of a joint connecting the mobile platform and a distal link, for which one Euler angle is identical to the arc subtended by the mid-curve of the distal links. The solution is given by the roots of an octic polynomial equation.

- *Using the actuated-joint angles as unknowns*

  This approach, adopted in [13], makes use of one of the three legs, for example, leg 1, for the expression of unit vectors $\mathbf{v}_i$, which are functions of the joints angles, i.e.,

$$\mathbf{v}_i = \mathbf{R}_i(\theta_1, \phi_1, \psi_1)\mathbf{v}_i^* \tag{6}$$

  For the FDA problem with known θ_1, only two unknowns per leg are present. By combining Eq. (1) for legs 2 and 3, a system of two equations for two variables is established. These equations lead finally to an octic polynomial equation.

Unlike the above methods, which directly rely on the single-leg Eq. (1), the method proposed here resorts to the input–output (I/O) equation of spherical four-bar linkages, upon consideration that the I/O equation is actually a combination of two closure equations of single individual legs. In this way, loop equations with compact coefficients can be expected, which may lead to less calculations and an enhanced robustness of the displacement analysis. Moreover, as shown in [16], the input–output equations of planar and spherical four-bar linkages can be expressed by a unified equation. Furthermore, because a SPR with prismatic joints is kinematically equivalent to a SPR with revolute joints, the method proposed here applies to the latter as well.

3. Forward-displacement analysis

In this section, we formulate the FDA equation in terms of the I/O equations of two spherical four-bar linkages.

3.1. I/O equation of a spherical four-bar linkage

The derivation of the I/O equation of spherical four-bar linkages is well documented in the literature [17,18]. We resort to the method proposed by Wampler [18], which we recall below for completeness.

Wampler's method is generally applicable to multi-loop spherical linkages. The idea is that the travel along a loop of a spherical mechanism consists of two types of rotations, namely, *joint rotations* and *side rotations*. The latter, which describe
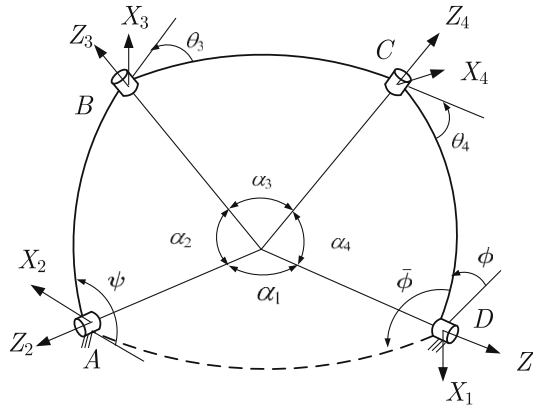
Fig. 3. The spherical four-bar loop: coordinate frames are established following D–H convention.

the relative orientation of every neighboring pair of joint axes of a link, are constant, while the former are variable. Referring to Fig. 3, the loop equation of the four-bar spherical linkage can be expressed as

$$\mathbf{Z}_4\mathbf{S}_4\mathbf{Z}_1\mathbf{S}_1\mathbf{Z}_2\mathbf{S}_2\mathbf{Z}_3\mathbf{S}_3 = \mathbf{I} \tag{7}$$

where $\mathbf{I}$ is the 3×3 identity matrix, while joint rotations are $\mathbf{Z}_1 = \mathbf{R}_z(\phi)$, $\mathbf{Z}_2 = \mathbf{R}_z(\pi - \psi)$, $\mathbf{Z}_3 = \mathbf{R}_z(\theta_3)$, and $\mathbf{Z}_4 = \mathbf{R}_z(\theta_4)$, with

$$\mathbf{R}_z(\cdot) = \begin{bmatrix} \cos(\cdot) & -\sin(\cdot) & 0 \\ \sin(\cdot) & \cos(\cdot) & 0 \\ 0 & 0 & 1 \end{bmatrix}$$

Moreover, side rotations are $\mathbf{S}_i = \mathbf{R}_x(\alpha_i), i = 1, \ldots, 4$, with

$$\mathbf{R}_x(\cdot) = \begin{bmatrix} 1 & 0 & 0 \\ 0 & \cos(\cdot) & -\sin(\cdot) \\ 0 & \sin(\cdot) & \cos(\cdot) \end{bmatrix}$$

Algebraic manipulation of Eq. (7) yields

$$\mathbf{z}^T\mathbf{S}_4\mathbf{Z}_1\mathbf{S}_1\mathbf{Z}_2\mathbf{S}_2\mathbf{z} = \mathbf{z}^T\mathbf{S}_3^T\mathbf{z} \tag{8}$$

with $\mathbf{z} = [0, 0, 1]^T$. Expanding Eq. (8) leads to

$$k_1 + k_2 \cos\psi + k_3 \cos\psi \cos\phi - k_4 \cos\phi + k_5 \sin\psi \sin\phi = 0 \tag{9a}$$

where

$$k_1 \equiv c\alpha_1 c\alpha_2 c\alpha_4 - c\alpha_3, \quad k_2 \equiv s\alpha_1 s\alpha_2 c\alpha_4, \quad k_3 \equiv c\alpha_1 s\alpha_2 s\alpha_4, \quad k_4 \equiv s\alpha_1 c\alpha_2 s\alpha_4, \quad k_5 \equiv s\alpha_2 s\alpha_4 \tag{9b}$$

and α_i denotes the ith-link dimension, the notation being valid for Fig. 3 only.

Introducing $\bar{\phi} = \pi - \phi$, the I/O equation with the $\{\psi, \bar{\phi}\}$ pair can be written as

$$k_1 + k_2 \cos\psi - k_3 \cos\psi \cos\bar{\phi} + k_4 \cos\bar{\phi} + k_5 \sin\psi \sin\bar{\phi} = 0 \tag{9c}$$

3.2. I/O equations for SPRs

A SPR essentially consists of several spherical loops. Two loops of spherical four-bar linkages, namely, $A_1C_1C_2A_2$ and $A_1C_1C_3A_3$, are selected for the ensuing analysis. Both loops have known link dimensions, if we consider arcs $\widehat{C_1C_2}$ and $\widehat{C_1C_3}$ as virtual links. For simplicity, the three legs have been assumed identical, i.e., $\alpha_{2,1} = \alpha_{2,2} = \alpha_{2,3} = \alpha_2$. The two loops selected in Fig. 4 fully determine a configuration of the SPR. Based on Eq. (9c), the I/O equation of the closed loop $A_1C_1C_2A_2$ with I/O pair $\{\psi, \phi\}$ is

$$c\alpha_2 c\alpha_3 c\alpha_4 - c\alpha_2 + s\alpha_2 s\alpha_3 c\alpha_4 c\psi - c\alpha_2 s\alpha_3 s\alpha_4 c\psi c\phi + s\alpha_2 c\alpha_3 s\alpha_4 c\phi + s\alpha_3 s\alpha_4 s\psi s\phi = 0 \tag{10a}$$

where $\alpha_4 = \angle C_1OC_2 = \cos^{-1}(\mathbf{w}_1 \cdot \mathbf{w}_2)$, $\alpha_4 \in (0, \pi]$. Eq. (10a) can be cast in the general form

$$A_1(\phi)c\psi + B_1(\phi)s\psi + C_1(\phi) = 0 \tag{10b}$$
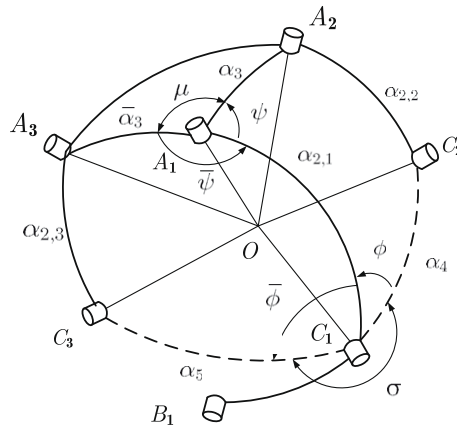
Fig. 4. Two spherical chains within a SPR with only leg 1 fully shown for clarity.

where

$$A_1 = s\alpha_2 s\alpha_3 c\alpha_4 - c\alpha_2 s\alpha_3 s\alpha_4 c\phi \tag{10c}$$

$$B_1 = s\alpha_3 s\alpha_4 s\phi \tag{10d}$$

$$C_1 = c\alpha_2 c\alpha_3 c\alpha_4 - c\alpha_2 + s\alpha_2 c\alpha_3 s\alpha_4 c\phi \tag{10e}$$

Likewise, the I/O equation for the $A_1C_1C_3A_3$ chain, with the I/O pair $\{\bar{\phi}, \bar{\psi}\}$, is obtained as

$$c\alpha_2 c\alpha_5 c\bar{\alpha}_3 + s\alpha_2 s\alpha_5 c\bar{\alpha}_3 c\bar{\phi} - c\alpha_2 s\alpha_5 s\bar{\alpha}_3 c\bar{\phi} c\bar{\psi} - c\alpha_2 + s\alpha_2 c\alpha_5 s\bar{\alpha}_3 c\bar{\psi} + s\alpha_5 s\bar{\alpha}_3 s\bar{\phi} s\bar{\psi} = 0 \tag{11a}$$

where $\cos\bar{\alpha}_3 = \mathbf{v}_1 \cdot \mathbf{v}_3$, $\bar{\alpha}_3 \in (0, \pi]$. Moreover, $\cos\alpha_5 = \mathbf{w}_1 \cdot \mathbf{w}_3$ and $\sin\alpha_5 = \|\mathbf{w}_1 \times \mathbf{w}_3\|$. The geometry of the SPR leads to the identities

$$\bar{\phi} = 2\pi - \phi - \sigma; \quad \bar{\psi} = 2\pi - \psi - \mu \tag{11b}$$

where σ is the dihedral angle between the planes C_1OC_3 and C_1OC_2, and μ is the spherical angle at vertex A_1. In the case of a mobile platform with an equilateral-triangular shape, μ takes the value

$$\mu = \cos^{-1}[\csc^2\alpha_3(\cos\alpha_3 - \cos^2\alpha_3)], \quad \mu \in (0, \pi] \tag{11c}$$

Substituting Eq. (11b) into Eq. (11a) and simplifying the equation thus resulting yields

$$A_2(\phi)c\psi + B_2(\phi)s\psi + C_2(\phi) = 0 \tag{11d}$$

with coefficients

$$A_2 = -c\alpha_2 s\alpha_5 s\bar{\alpha}_3 c\sigma c\mu c\phi + c\alpha_2 s\alpha_5 s\bar{\alpha}_3 s\sigma c\mu s\phi + s\alpha_2 c\alpha_5 s\bar{\alpha}_3 c\mu + s\alpha_5 s\bar{\alpha}_3 c\sigma s\mu s\phi + s\alpha_5 s\bar{\alpha}_3 s\sigma s\mu c\phi \tag{11e}$$

$$B_2 = c\alpha_2 s\alpha_5 s\bar{\alpha}_3 c\sigma s\mu c\phi - c\alpha_2 s\alpha_5 s\bar{\alpha}_3 s\sigma s\mu s\phi - s\alpha_2 c\alpha_5 s\bar{\alpha}_3 s\mu + s\alpha_5 s\bar{\alpha}_3 c\sigma c\mu s\phi + s\alpha_5 s\bar{\alpha}_3 s\sigma c\mu c\phi \tag{11f}$$

$$C_2 = c\alpha_2 c\alpha_5 c\bar{\alpha}_3 - c\alpha_2 + s\alpha_2 s\alpha_5 c\bar{\alpha}_3 c\sigma c\phi - s\alpha_2 s\alpha_5 c\bar{\alpha}_3 s\sigma s\phi \tag{11g}$$

3.3. Semigraphical equation solving

Both Eqs. (10b) and (11d) are linear in $[\cos\psi, \ \sin\psi]^T$, whence

$$\cos\psi = \frac{1}{\Delta}(B_1 C_2 - B_2 C_1); \quad \sin\psi = \frac{1}{\Delta}(A_1 C_2 - A_2 C_1), \quad \Delta \equiv A_1 B_2 - A_2 B_1 \tag{12}$$

Below we consider two cases, depending on the vanishing of the denominator appearing in Eq. (12).

3.3.1. General case

Assuming $\Delta \neq 0$ and adding sidewise the squares of Eq. (12) yields

$$C_2^2 A_1^2 + 2A_2 B_2 A_1 B_1 - 2A_2 C_2 A_1 C_1 + C_2^2 B_1^2 - A_2^2 B_1^2 - 2B_2 C_2 B_1 C_1 - B_2^2 A_1^2 + A_2^2 C_1^2 + B_2^2 C_1^2 = 0 \tag{13}$$

which, in light of Eq. (11e–g), involves powers of $\sin\phi$ and $\cos\phi$ only. The real roots of the equation can be obtained semigraphically, as described presently.

Substituting $x = \cos\phi$ and $y = \sin\phi$ into Eq. (13) yields

$$f(x, y) = 0 \tag{14}$$

which is a quartic equation in (x, y). Moreover, x and y are subject to the constraint

$$x^2 + y^2 = 1 \tag{15}$$

To solve the system of Eqs. (14) and (15) semigraphically, first the two equations are plotted and all intersections are estimated by inspection. There are at most eight intersections, which yield as many rough estimates $\{\hat{x}_i, \hat{y}_i\}_1^8$ of the solutions. Second, the rough estimates are submitted as initial guesses to a nonlinear-equation solver for accurate solution.

It is noted that Eq. (13) can also be solved by making use of the tan-half identities, as reported in [12], which yields an octic polynomial, the robot *characteristic polynomial*, namely,

$$\sum_{i=0}^{8} N_i t^i = 0, \quad t = \tan(\phi/2) \tag{16}$$

whose coefficients N_i appear in terms of all known parameters. However, the computation with tan-half identities becomes ill-conditioned if $\phi \to \pi$ [19], which leads to $t \to \infty$. For this reason, we resort to the semigraphical method, as described above.

It is worth comparing this method with that reported in [12] and highlight their differences. While both methods yield a trigonometric equation of the form of Eq. (13), they involve totally different expressions for its coefficients. The method reported here, utilizing the I/O Eqs. (10b) and (11d), leads to the compact coefficients displayed in Eqs. (10c–e) and (11e–g). Taking the coefficient A_1 as an example, this consists of only two terms in our method, while its counterpart in [12] consists of 29 terms of trigonometric products, namely,

$$
\begin{aligned}
(A_1)_{[12]} = &-\frac{\sqrt{3}}{2}s\alpha_1 c\gamma_1 c\theta_2 s\theta_1 c\alpha_1 s\alpha_3 c\alpha_2 c\phi_1 - \frac{3}{2}s\gamma(c\alpha_1)^2 c\gamma c\theta_1 s\alpha_3 c\alpha_2 c\phi_1 - \frac{\sqrt{3}}{2}(s\alpha_1)^2 s\theta_2 s\gamma s\alpha_3 c\alpha_2 c\phi_1 \\
&-\frac{1}{2}s\alpha_1 s\theta_2 s\theta_1 c\alpha_1 s\alpha_3 c\alpha_2 c\phi_1 - \frac{\sqrt{3}}{2}s\gamma(c\alpha_1)^2 s\theta_1 s\alpha_3 c\alpha_2 c\phi_1 - (c\gamma)^2 c\alpha_1 s\alpha_1 s\alpha_3 c\alpha_2 c\phi_1 \\
&+\frac{\sqrt{3}}{2}s\alpha_1 s\theta_2 c\gamma c\theta_1 c\alpha_1 s\alpha_3 c\alpha_2 c\phi_1 + \frac{1}{2}(s\gamma)^2 c\alpha_1 s\alpha_1 s\alpha_3 c\alpha_2 c\phi_1 - \frac{1}{2}s\alpha_1 (c\gamma)^2 c\theta_2 c\theta_1 c\alpha_1 s\alpha_3 c\alpha_2 c\phi_1 \\
&+(s\gamma)^2 c\theta_2 s\alpha_1 c\theta_1 c\alpha_1 s\alpha_3 c\alpha_2 c\phi_1 + \frac{3}{2}(s\alpha_1)^2 c\gamma c\theta_2 s\gamma s\alpha_3 c\alpha_2 c\phi_1 - \frac{\sqrt{3}}{2}s\alpha_1 c\gamma c\theta_2 c\theta_1 s\alpha_3 c\alpha_2 s\phi_1 \\
&-\frac{1}{2}s\alpha_1 s\theta_2 c\theta_1 s\alpha_3 c\alpha_2 s\phi_1 + \frac{1}{2}s\alpha_1 (c\gamma)^2 c\theta_2 s\theta_1 s\alpha_3 c\alpha_2 s\phi_1 + \frac{3}{2}s\gamma c\alpha_1 c\gamma s\theta_1 s\alpha_3 c\alpha_2 s\phi_1 \\
&-\frac{\sqrt{3}}{2}s\gamma c\alpha_1 c\theta_1 s\alpha_3 c\alpha_2 s\phi_1 - \frac{\sqrt{3}}{2}s\alpha_1 s\theta_2 c\gamma_1 s\theta_1 s\alpha_3 c\alpha_2 s\phi_1 - (s\gamma)^2 c\theta_2 s\alpha_1 s\theta_1 s\alpha_3 c\alpha_2 s\phi_1 \\
&+\frac{3}{2}s\gamma c\alpha_1 c\gamma c\theta_1 s\alpha_1 s\alpha_2 s\alpha_3 - \frac{\sqrt{3}}{2}s\alpha_1 s\theta_2 s\gamma_1 c\alpha_1 s\alpha_2 s\alpha_3 - \frac{\sqrt{3}}{2}(s\alpha_1)^2 s\theta_2 c\gamma c\theta_1 s\alpha_2 s\alpha_3 \\
&+\frac{1}{2}(s\gamma)^2 (c\alpha_1)^2 s\alpha_2 s\alpha_3 + \frac{3}{2}s\alpha_1 c\gamma c\theta_2 s\gamma c\alpha_1 s\alpha_2 s\alpha_3 - (c\gamma_1)^2 (c\alpha_1)^2 s\alpha_2 s\alpha_3 + \frac{\sqrt{3}}{2}(s\alpha_1)^2 c\gamma c\theta_2 s\theta_1 s\alpha_2 s\alpha_3 \\
&+\frac{1}{2}(s\alpha_1)^2 (c\gamma_1)^2 c\theta_2 c\theta_1 s\alpha_2 s\alpha_3 + \frac{\sqrt{3}}{2}s\gamma c\alpha_1 s\theta_1 s\alpha_1 s\alpha_2 s\alpha_3 \\
&+\frac{1}{2}(s\alpha_1)^2 s\theta_2 s\theta_1 s\alpha_2 s\alpha_3 - (s\gamma)^2 c\theta_2 (s\alpha_1)^2 c\theta_1 s\alpha_2 s\alpha_3 \tag{17}
\end{aligned}
$$

which was derived for a SPR of symmetric architecture with identical legs. Coefficients B_1, C_1, A_2, B_2 and C_2 of Eqs. (10d&e) and (11e–g), respectively, bear 1, 3, 5, 5, and 4 terms, respectively, of trigonometric products in our method, compared with 18, 36, 47, 49, and 35 terms for their counterparts in [12]. As a matter of fact, the coefficients in [12] are so long that they were not included in that paper. Compact coefficients not only facilitate implementation, but also enhance the accuracy of computations, as the number of flops is dramatically reduced.

Once the real roots of Eq. (13) are found, the corresponding solutions of ψ are uniquely determined through Eq. (12). Moreover, the three vectors $\mathbf{v}_1, \mathbf{v}_2,$ and $\mathbf{v}_3$ can be readily calculated from Eq. (4), in which the rotation matrix now becomes

$$\mathbf{Q} = \mathbf{R}_x(\gamma - \pi/2)\mathbf{R}_z(\theta_1)\mathbf{R}_x(\alpha_1)\mathbf{R}_z(\pi - \phi_1)\mathbf{R}_x(\alpha_2)\mathbf{R}_z(\psi) \tag{18}$$

where

$$\phi_1 = \phi + \phi_0 \tag{19}$$

with ϕ_0 denoting the dihedral angle between the $C_1 O C_2$ and $C_1 O B_1$ planes, which can be found unambiguously from the relations

$$\cos \phi_0 = \mathbf{n}_a \cdot \mathbf{n}_b; \quad \sin \phi_0 = \|\mathbf{n}_a \times \mathbf{n}_b\| \tag{20}$$

with

$$\mathbf{n}_a = \frac{\mathbf{w}_3 \times \mathbf{w}_1}{\|\mathbf{w}_3 \times \mathbf{w}_1\|}; \quad \mathbf{n}_b = \frac{\mathbf{u}_1 \times \mathbf{w}_1}{\|\mathbf{u}_1 \times \mathbf{w}_1\|} \tag{21}$$

3.3.2. Particular case

As shown in [16], the vanishing of the denominator of Eq. (12) leads to $C_1 = C_2 = 0$, the right-hand sides of the first two of Eq. (12) thus leading to an indeterminacy. In fact, the vanishing of C_1 and C_2 also leads to the vanishing of the denominator Δ of Eq. (12). To find solutions of ψ and ϕ in this case, we let Eq. (14) take the form of the condition itself, i.e., $\Delta = 0$, which leads to solutions of ϕ by following the same semigraphical approach. These solutions will be substituted into one of the two Eqs. (10b) and (11d) to obtain a linear homogenous equation in $\sin\psi$ and $\cos\psi$, each equation leading to two values of ψ.

As shown in the examples, an interesting particular case is that in which the robot has identical proximal and distal links. In this case, an architectural singularity occurs, as the four-bar linkage becomes *foldable* [20]. Moreover, the link dimensions are identical to the angles made by adjacent joint axes on the mobile platform.

So far, we have developed a method for the FDA solutions of SPRs with revolute joints. Note that the method developed is readily applicable to SPRs with prismatic joints, once they are converted to their equivalent models with revolute joints, as described in Appendix A.

4. Examples

We include three examples to demonstrate the application of the method reported here in determining the orientation of the mobile platform and the analysis of the assembly modes of SPRs. The FDA of a robot prototype is also included.

4.1. Example 1: Determination of the directions of the joint axes

This example is given for the SPR with three identical legs and dimensions given as $\alpha_1 = 45°$, $\alpha_2 = 90°$, $\beta = 60°$ and $\gamma = 45°$, with reference to Fig. 2. The input angles are $\theta_1 = 105°$, $\theta_2 = 60°$ and $\theta_3 = 105°$. Each input angle is measured from the plane made by the z axis and $\mathbf{u}_i$.

In determining the unit vectors $\mathbf{v}_i$ of the joint axes on the mobile platform, we need first to find all unit vectors $\mathbf{u}_i$ and $\mathbf{w}_i$. The unit vectors $\mathbf{u}_i$ for the revolute joints on the base platform are readily given as:

$$\mathbf{u}_i = [-\sin\eta_i \sin\gamma, \quad \cos\eta_i \sin\gamma, \quad -\cos\gamma]^T, \quad i = 1, 2, 3 \tag{22}$$

where η_i is the angle measured from the plane made by the z axis and $\mathbf{u}_1$ to the plane made by the z axis and $\mathbf{u}_i$. As the SPR has a symmetric structure, $\eta_i = 2(i-1)\pi/3$.

Each unit vector $\mathbf{w}_i$, $i = 1, 2, 3$, is a function of the corresponding actuated-joint angle, which can be expressed as

$$\mathbf{w}_i = \mathbf{w}_i(\theta_i) \tag{23}$$

An explicit expression of $\mathbf{w}_i$ is

$$\mathbf{w}_i = \begin{bmatrix} -s\eta_i s\gamma c\alpha_1 + (c\eta_i s\theta_i - s\eta_i c\gamma c\theta_i)s\alpha_1 \\ c\eta_i s\gamma c\alpha_1 + (s\eta_i s\theta_i + c\eta_i c\gamma c\theta_i)s\alpha_1 \\ -c\gamma c\alpha_1 + s\gamma c\theta_i s\alpha_1 \end{bmatrix} \tag{24}$$

With fixed dimensions and the joint angles θ_i, for $i = 1, 2, 3$, given above, the unit vectors $\mathbf{w}_i$ are calculated first through Eq. (24). The values of α_4 and α_5 are found as $\alpha_4 = 2.024$ rad and $\alpha_5 = 1.514$ rad. Once all the dimensions of the two closed-loop chains are known, Eq. (14) becomes

$$0.012174x^4 + 0.0030528x^3y - 0.75454x^2y^2 - 0.16791xy^3 + 0.0031315y^4 + 0.0012876x^3 + 0.094285x^2y$$
$$+ 0.040248xy^2 + 0.0035373y^3 - 0.0035850x^2 + 0.066951xy + 0.010187y^2 - 0.0048985x - 0.0014952y$$
$$- 0.0016159 = 0 \tag{25}$$

where $x = \cos\phi$, $y = \sin\phi$. The curve defined by this equation and the unit circle are displayed in Fig. 5. The eight intersections lead to the eight solutions of $[\cos\phi, \sin\phi]^T$. Based on the estimated coordinates of the intersecting points, more accurate results were obtained with the nonlinear-equation solver available in Maple 10. It is noted that the dashed curves in Fig. 5 are plots of $A_1B_2 - A_2B_1 = 0$. It is also noted that there are no common points between this curve and the eight solutions, which means that the right-hand sides of Eq. (12) are computed safely.

With the eight values of ϕ, the corresponding solutions of ψ are further found through Eq. (12). The eight pairs of values of ψ and ϕ are recorded in Table 1. The angle of the middle joint at leg 1 is then determined from Eq. (19). The unit vectors $\mathbf{v}_i$ are finally calculated via Eqs. (4) and (18), and recorded in Table 2.

The computation error is defined as

$$\varepsilon = \sqrt{\frac{1}{24} \sum_{j=1}^{8} \sum_{i=1}^{3} [\mathbf{w}_i \cdot \mathbf{v}_i(\phi_j, \psi_j) - \cos\alpha_2]^2} \tag{26}$$

The error with the reported method is 4.5×10^{-6}, while the error with the method in [12] is found as 9.1×10^{-6}. The improvement here is not dramatic, but still noticeable.
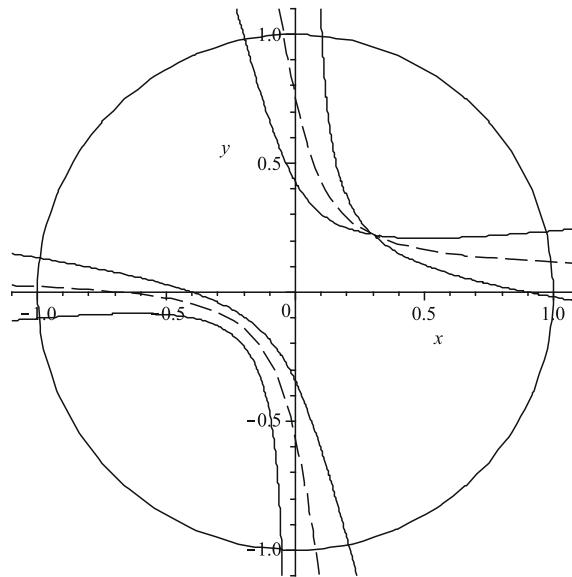
Fig. 5. Curve plot to find eight intersections.

Table 1
The eight real solutions of Example 1.

No.	1	2	3	4	5	6	7	8
ψ [rad]	1.52083	2.6818	−0.485793	−1.79311	1.34851	−2.69801	0.438398	−1.58601
ϕ [rad]	−3.04028	−1.62406	−1.36202	−0.0190524	0.237828	1.46761	1.76812	3.00891

Table 2
The eight forward-displacement solutions of Example 1.

No.	$\mathbf{v}_1^T$	$\mathbf{v}_2^T$	$\mathbf{v}_3^T$
1	[0.72606, −0.43833, 0.52981]	[0.021926, 0.88458, 0.46583]	[−0.77283, −0.38699, 0.50298]
2	[0.03320, −0.87656, −0.48006]	[−0.29015, −0.35510, 0.88866]	[−0.90301, 0.28461, −0.32176]
3	[−0.15699, −0.76706, −0.62198]	[0.28844, 0.66362, −0.69024]	[0.91383, −0.27000, 0.30330]
4	[−0.73034, 0.33682, −0.59424]	[−0.06608, 0.71447, 0.69650]	[0.76616, 0.39220, −0.50905]
5	[−0.70846, 0.54568, −0.44752]	[0.06607, −0.71449, −0.69650]	[−0.60086, −0.49359, 0.62874]
6	[−0.06955, 0.89082, 0.44903]	[−0.29376, −0.55540, 0.77796]	[0.98460, −0.12493, 0.12199]
7	[0.14878, 0.77306, 0.61662]	[0.29378, 0.45310, −0.84165]	[−0.98370, 0.12812, −0.12596]
8	[0.72469, −0.23653, 0.64717]	[−0.010662, −0.86701, −0.49807]	[0.56997, 0.50807, −0.64575]

4.2. Example 2: analysis of assembly modes

The FDA is needed in the analysis of assembly modes. In this example, the eight assembly modes are examined with the FDA solutions. The SPR shown in Fig. 6 is a special robot with coaxial input shafts, which means $\gamma = 0$. Moreover, $\mathbf{u}_1 = \mathbf{u}_2 = \mathbf{u}_3 = [0, 0, 1]^T$. This SPR features unlimited rolling, which makes the SPR capable of being used as an actuated spherical joint in robotic applications [21].

The dimensions of the SPR are given as $\alpha_1 = 45°$, $\alpha_2 = 90°$, and $\beta = 60°$. At the initial position with the angular displacements of all input shafts equal to zero, i.e., $\theta_i = 0$, $i = 1, 2, 3$, the eight solutions of the forward-displacement problem are found as listed in Table 3. Based on these solutions, all eight postures are displayed in Fig. 7. We calculated for each posture the conditioning index *CI*, which is defined as the reciprocal of the condition number of the Jacobian $\mathbf{J}$ [22], i.e.,

$$CI = 1/\kappa = 1/(\|\mathbf{J}^{-1}\|\|\mathbf{J}\|) \tag{27}$$

where $\|\cdot\|$ denotes the Frobenius norm of $\mathbf{J}$, namely,

$$\|\mathbf{J}\| = \sqrt{\text{tr}(\mathbf{J}^T\mathbf{W}\mathbf{J})} \tag{28}$$

with $\mathbf{W} = (1/3)\mathbf{I}$, and $\mathbf{I}$ having been defined earlier as the 3×3 identity matrix.
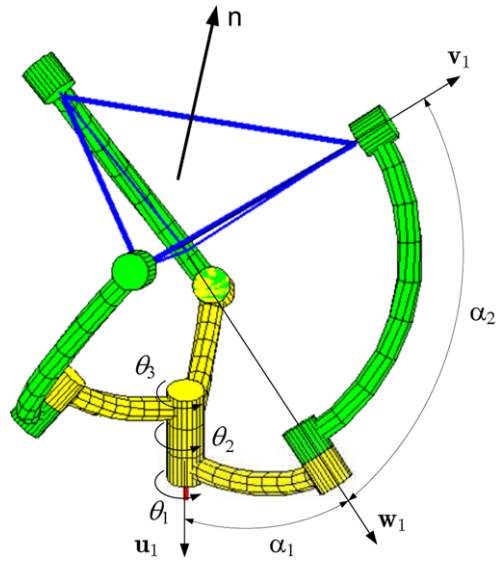
Fig. 6. Model of a spherical parallel robot with coaxial input shafts.

Table 3
Eight forward-displacement solutions for Example 2.

No.	$\mathbf{v}_1^T$	$\mathbf{v}_2^T$	$\mathbf{v}_3^T$
1	[−0.6494,−0.5377,−0.5377]	[0.76948,−0.06107,−0.63575]	[0.28874,−0.73259,0.61635]
2	[−0.70711,0.5,0.5]	[−0.079461,−0.86235,0.49999]	[0.78656,0.36233,0.50003]
3	[−0.4901,0.61635,0.61635]	[0.33185,0.69686,−0.6358]	[−0.79038,−0.29356,−0.53772]
4	[0.4901,0.61635,0.61635]	[0.79038,−0.29356,−0.53772]	[−0.33183,0.69686,−0.6358]
5	[−0.43757,−0.6358,−0.6358]	[−0.77886,0.11627,0.61633]	[−0.14094,0.83129,−0.53769]
6	[0.43758,−0.6358,−0.6358]	[0.1409,0.83127,−0.53771]	[0.77885,0.11627,0.61633]
7	[0.64949,−0.53765,−0.53765]	[−0.28873,−0.73261,0.61633]	[−0.76941,−0.06112,−0.6358]
8	[0.7071,0.5,0.5]	[−0.78658,0.36239,0.49997]	[0.079402,−0.86236,0.50008]
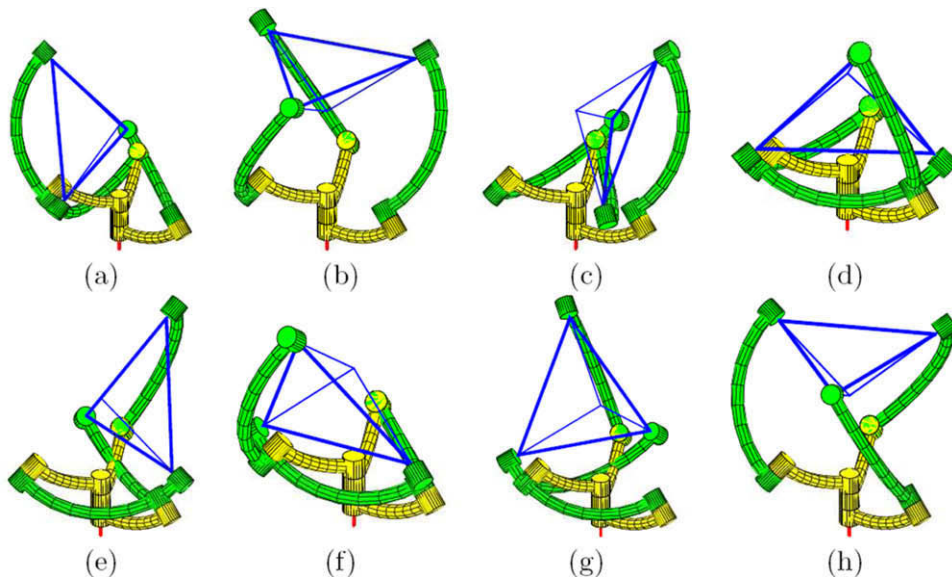
Fig. 7. Eight postures of a SPR with coaxial input shafts, as produced by $\theta_1 = \theta_2 = \theta_3 = 0$.

The Jacobian matrix of SPRs can be obtained upon differentiation of Eq. (1), which gives

$$\dot{\mathbf{w}}_i \cdot \mathbf{v}_i + \mathbf{w}_i \cdot \dot{\mathbf{v}}_i = 0 \tag{29a}$$

Table 4
Conditioning indices (CI) of the eight postures for Example 2.

Posture	a	b	c	d	e	f	g	h
CI	0.821	0.982	0.821	0.821	0.821	0.821	0.821	0.982
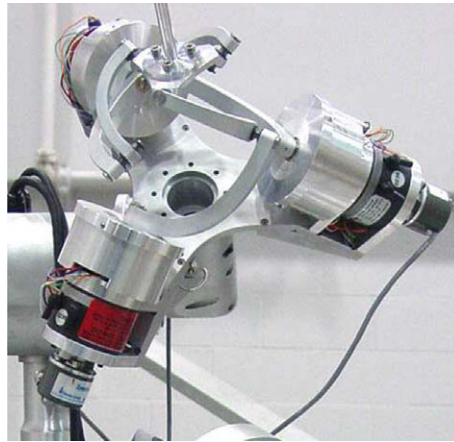
Fig. 8. Prototype of the Agile Wrist.
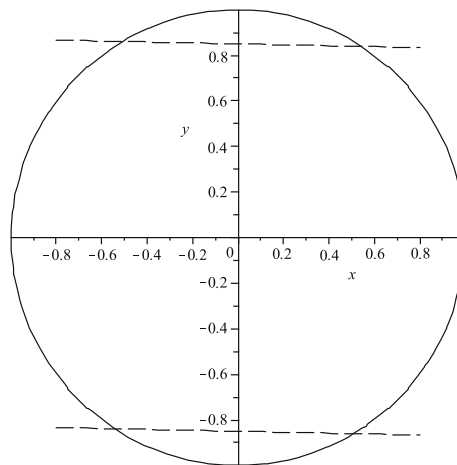
Fig. 9. Curve plot to find the solutions of a particular case.

Table 5
Eight forward-displacement solutions for Example 3.

No.	$\mathbf{v}_1^T$	$\mathbf{v}_2^T$	$\mathbf{v}_3^T$
1	[0.27657,0.12704,0.95259]	[0.54651,0.79457,−0.26459]	[−0.79047,0.59378,0.15034]
2	[0.27657,0.12704,0.95259]	[−0.54652,−0.79457,0.26459]	[0.79047,−0.59379,−0.15034]
3	[0,−0.81649,0.57736]	[0.7071,0.40826,0.57738]	[−0.70712,0.40825,0.57737]
4	[0,−0.81649,0.57736]	[−0.70711,−0.40826,−0.57738]	[0.7071,−0.40826,−0.57737]
5	[−0.27656,−0.1269,−0.95264]	[−0.54654,−0.79459,0.26453]	[−0.79046,0.5938,0.15038]
6	[−0.27656,−0.1269,−0.95264]	[0.54653,0.79459,−0.26453]	[0.79046,−0.59379,−0.15039]
7	[0,0.81649,−0.57737]	[−0.70711,−0.40827,−0.57738]	[−0.7071,0.40826,0.57737]
8	[0,0.81649,−0.57737]	[0.7071,0.40827,0.57738]	[0.70712,−0.40825,−0.57737]

Note that

$$\dot{\mathbf{v}}_i = \boldsymbol{\omega} \times \mathbf{v}_i, \quad \dot{\mathbf{w}}_i = \mathbf{u}_i \times \mathbf{w}_i \dot{\theta}_i, \tag{29b}$$
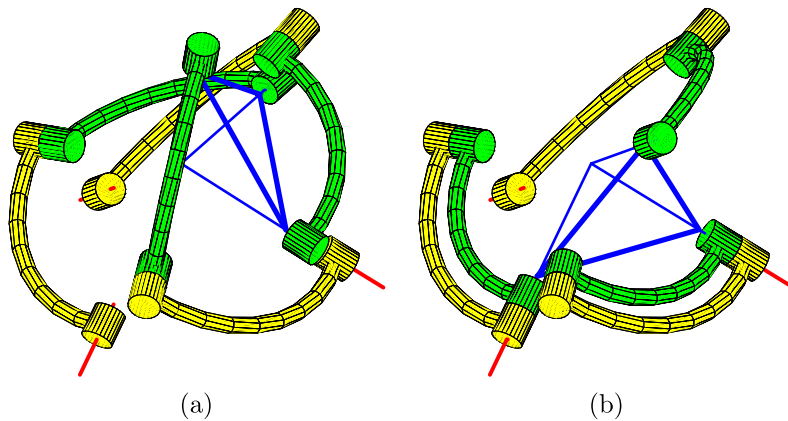
Fig. 10. Two possible configurations of the Agile Wrist: (a) a regular configuration and (b) a singular configuration.

where ω is the angular-velocity vector of the mobile platform. Eq. (29a and b) lead to

$$\mathbf{J}\omega = \dot{\theta} \tag{30}$$

where

$$\mathbf{J} = [\mathbf{j}_1, \mathbf{j}_2, \mathbf{j}_3], \quad \mathbf{j}_i = \frac{\mathbf{w}_i \times \mathbf{v}_i}{(\mathbf{u}_i \times \mathbf{w}_i) \cdot \mathbf{v}_i} \tag{31}$$

The conditioning indices of all assembly modes are shown in Table 4. It is found that postures (b) and (h) have an identical conditioning index, which is equal to 0.982, larger than the other configurations. In view of this, the home posture can be selected as one of the two modes, (b) and (h).

The method was also used for the FDA of a SPR with prismatic joints, taking data from the example given in [11]. FDA solutions were obtained that are in full agreement with the results reported in [11].

4.3. Example 3: FDA of the agile eye/wrist

In this example, we apply the method developed here to the FDA of the *Agile Wrist*, a spherical parallel robot developed at the Centre for Intelligent Machines, McGill University, as shown in Fig. 8. The kinematic chain of the Agile Wrist was borrowed from the design of the Agile Eye, developed at Laval University in Quebec City [1]. The robot was redesigned in order to enhance its load-carrying capacity, while minimizing its weight [23,24].

The dimensions of the Agile Wrist are $\alpha_1 = \alpha_2 = \pi/2$, all three legs being identical. Moreover, the three unit vectors $\mathbf{u}_i$ are mutually orthogonal, vectors $\mathbf{v}_i$, $i = 1, 2, 3$, following suit. It can be found from Eqs. (10e) and (11g) that $C_1 = C_2 = 0$, which implies $\Delta = 0$. Hence, the method of (3.3.2) applies. A FDA example is given for $\theta_1 = 3\pi/5, \theta_2 = \pi/3, \theta_3 = 7\pi/12$. The plot for Eq. (14) is shown in Fig. 9. Altogether, eight forward-displacement solutions are found, as recorded in Table 5. Of them, four corresponding configurations are regular, four are singular. Two configurations, one regular and one singular, are shown in Fig. 10. For singular configurations, the angles of rotation of the middle joints are either zero or 180°, the axes of the revolute joints at the mobile platform are thus parallel to their counterparts on the fixed platform. Hence, the rotations of the input shafts cannot control the orientation of the mobile platform. This type of singularity is the input singularity discussed in [20]. For this reason, the four singular solutions can be identified by means of the singularity of the relevant Jacobian. In the given example, solutions 3, 4, 7 and 8 are singular.

It is noted that the singular solutions correspond to the *pathological cases* of four-bar linkages [16], if we look at the loops of the mechanism. Due to the special nature of the solutions, the method reported in [12] is not applicable to this example. It is also noted that these singular solutions are the trivial solutions analyzed in [25].

5. Conclusions

The forward-displacement analysis of spherical parallel robots was revisited in this paper. A robust method to determine the orientation of the end-effector is developed using the I/O equations of spherical four-bar linkages. With the proposed method, the FDA equations are derived with compact coefficients, which leads to a robust procedure. Moreover, a semi-graphical method is applied to equation-solving, which contributes to the robustness of the displacement analysis. The method is able to handle general FDA cases as well as particular cases involving singularities.

Examples are included to demonstrate the application of the proposed method. The improvement of calculation accuracy is noticeable. The method can be used in the forward-displacement analysis and the working-mode analysis of SPRs
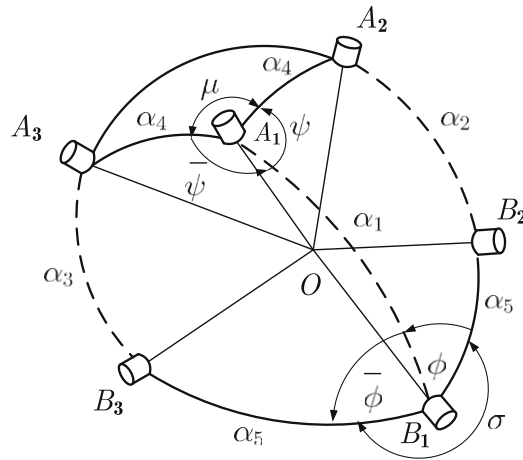
Fig. 11. Equivalent revolute-coupled chain of a SPR with prismatic joints.

consisting of different types of joints. The method should also be applied to the FDA of other types of parallel robots for which input–output equations of similar forms can be established.

Appendix A. The FDA of SPRs with P-joints

A SPR with prismatic joints is kinematically equivalent to a revolute-coupled SPR. Fig. 11 shows the equivalent model of the SPR of Fig. 1bb. Dimensions $\alpha_i, i = 1, 2, 3$, are found from relations

$$\cos \alpha_i = \frac{r_{a,i}^2 + r_{b,i}^2 - l_i^2}{2r_{a,i}r_{b,i}}, \quad \alpha_i \in (0, \pi], \; i = 1, 2, 3 \tag{32}$$

while α_4 and α_5 are angles pertaining to the mobile and fixed pyramids, respectively. Moreover, $r_{a,i}$ and $r_{b,i}$ are the lengths of A_iO and B_iO, respectively, for the original model depicted in Fig. 1b.

Two loops, $A_1B_1B_2A_2$ and $A_1B_1B_3A_3$, as shown in Fig. 11 are selected for the analysis. With reference to Eq. (9c), the I/O equations of the two loops are

$$A_1(\phi)c\psi + B_1(\phi)s\psi + C_1(\phi) = 0 \tag{33a}$$
$$A_2(\phi)c\psi + B_2(\phi)s\psi + C_2(\phi) = 0 \tag{33b}$$

with coefficients

$$A_1 = s\alpha_1 c\alpha_5 s\alpha_4 - c\alpha_1 s\alpha_5 s\alpha_4 c\phi, \quad B_1 = s\alpha_5 s\alpha_4 s\phi, \quad C_1 = c\alpha_1 c\alpha_5 c\alpha_4 - c\alpha_2 + s\alpha_1 s\alpha_5 c\alpha_4 s\phi \tag{33c}$$
$$A_2 = -c\alpha_1 s\alpha_5 s\alpha_4 c\sigma c\mu c\phi + c\alpha_1 s\alpha_5 s\alpha_4 s\sigma c\mu s\phi + s\alpha_1 c\alpha_5 s\alpha_4 c\mu + s\alpha_5 s\alpha_4 c\sigma s\mu s\phi + s\alpha_5 s\alpha_4 s\sigma s\mu c\phi \tag{33d}$$
$$B_2 = c\alpha_1 s\alpha_5 s\alpha_4 c\sigma s\mu c\phi - c\alpha_1 s\alpha_5 s\alpha_4 s\sigma s\mu s - s\alpha_1 c\alpha_5 s\alpha_4 s\mu + s\alpha_5 s\alpha_4 c\sigma c\mu s\phi + s\alpha_5 s\alpha_4 s\sigma c\mu c\phi \tag{33e}$$
$$C_2 = c\alpha_1 c\alpha_5 c\alpha_4 - c\alpha_3 + s\alpha_1 s\alpha_5 c\alpha_4 c\sigma c\phi - s\alpha_1 s\alpha_5 c\alpha_4 s\sigma s\phi \tag{33f}$$

It is noted that Eqs. (33a) and (33b) have the same gestalt as Eqs. (10b) and (11d). Thus, the procedure applied to the 3-RRR SPR can be followed here to obtain all real solutions. Upon finding these solutions, first for ϕ, and then for ψ, the unit vectors $\mathbf{v}_i$ are readily calculated.

References

[1] C.M. Gosselin, J.F. Hamel, The Agile Eye: a high-performance three-degree-of-freedom camera-orienting device, in: IEEE International Conferecne on Robotics and Automation, 1994, pp. 781–786.
[2] T. Li, S. Payandeh, Design of spherical parallel mechanisms for application to laparoscopic surgery, Robotica 20 (2) (2002) 133–138.
[3] W.M. Craver, D. Tesar, Force and deflection determination for a parallel three degree of freedom robotic shoulder module, in: ASME 1990 Design Technical Conferences, 1990, pp. 473–479.
[4] C.M. Gosselin, J. Angeles, The optimum kinematic design of a spherical three-degree-of-freedom parallel manipulator, ASME J. Mech., Transm. Automat. Des. 111 (1989) 202–207.
[5] S. Leguay-Durand, C. Reboulet, Optimal design of a redundant spherical parallel manipulator, Robotica 15 (4) (1997) 399–405.
[6] H. Asada, J. Granito, Kinematic and static characterization of wrist joints and their optimal design, in: IEEE International Conference on Robotics and Automation, 1985, pp. 244–250.
[7] P.M. Larochelle, Design of 3-dof spherical robotic mechanisms, in: Ninth IFToMM World Congress on the Theory of Machines and Mechanisms, Milan, Itali, 1995.

[8] X.J. Liu, Z.L. Jin, F. Gao, Optimum design of 3-DOF spherical parallel manipulators with respect to the conditioning and stiffness indices, Mech. Mach. Theory 35 (9) (2000) 1257–1267.

[9] C.M. Gosselin, J. Wang, Singularity loci of a special class of spherical three-degree-of-freedom parallel mechanisms with revolute actuators, Int. J. Robot. Res. 21 (7) (2002) 649–659.

[10] X. Kong, C.M. Gosselin, Type synthesis of three-degree-of-freedom spherical parallel manipulators, Int. J. Robot. Res. 23 (3) (2004) 237–245.

[11] C. Innocenti, V. Parenti-Castelli, Echelon form solution of direct kinematics for the general fully-parallel spherical wrist, Mech. Mach. Theory 28 (1993) 553–561.

[12] C.M. Gosselin, J. Sefrioui, M.J. Richard, On the direct kinematics of spherical three-degree-of-freedom parallel manipulators of general architecture, ASME J. Mech. Des. 116 (2) (1994) 594–598.

[13] Z. Huang, Y.L. Yao, A new closed-form kinematics of the generalized 3-dof spherical parallel manipulator, Robotica 17 (5) (1999) 475–485.

[14] R.I. Alizade, N.R. Tagiyiev, J. Duffy, A forward and reverse displacement analysis of an in-parallel spherical manipulator, Mech. Mach. Theory 29 (1) (1994) 125–137.

[15] P. Ji, H. Wu, Algebraic solution to forward kinematics of 3-DOF spherical parallel manipulator, Journal of Robotic Systems 18 (5) (2001) 251–257.

[16] S. Bai, J. Angeles, A unified input–output analysis of four-bar linkages, Mech. Mach. Theory 43 (2) (2008) 240–251.

[17] A. Yang, F. Freudenstein, Application of dual-number quaternion algebra to the analysis of spatial mechanisms, Journal of Applied Mechanics 31 (1964) 300–307.

[18] C.W. Wampler, Displacement analysis of spherical mechanisms having three or fewer loops, in: Proceedings 2002 ASME Design Engineering Technical Conferences, 2002, pp. 1075–1085.

[19] G.E. Forsythe, Pitfalls in computation, or why a math book isn't enough, American Mathematical Monthly 27 (1970) 931–956.

[20] C.M. Gosselin, J. Angeles, Singularity analysis of closed-loop kinematic chains, IEEE Trans. Robot. Automat. 6 (3) (1990) 281–290.

[21] S. Bai, M.R. Hansen, T.O. Andersen, Modelling of a special class of spherical parallel manipulators with Euler parameters, Robotica 27 (2) (2009) 161–170.

[22] J-P Merlet, Jacobian, manipulability, condition number, and accuracy of parallel robots, ASME J. Mech. Des. 128 (1) (2006) 199–206.

[23] F. Bidault, C.P. Teng, J. Angeles, Structural optimization of a spherical parallel manipulator using a two-level approach, in: Proceedings of ASME 2001 Design Engineering Technical Conferences, 2001.

[24] C.P. Teng, S. Bai, J. Angeles, Shape synthesis in mechanical design, Acta Polytechnica 47 (6) (2007) 56–62.

[25] I.A. Bonev, D. Chablat, P. Wenger, Working and assembly modes of the agile eye, in: IEEE International Conference on Robotics and Automation, 2006, pp. 2317–2322.